Materials Today Bio 19 (2023) 100575

Contents lists available at ScienceDirect

Materials Today Bio

journal homepage: www.journals.elsevier.com/materials-today-bio

Triton modified polyethyleneimine conjugates assembled with growth arrest-specific protein 6 for androgenetic alopecia transdermal gene therapy

Xinli Fan [a], Xiaoran Zhao [a], Jianfei Xu [a], Jing Wang [a], Qian Wang [a], Xinjing Tang [a,b,*]

[a] State Key Laboratory of Natural and Biomimetic Drugs, School of Pharmaceutical Sciences and Chemical Biology Center, and Beijing Key Laboratory of Molecular Pharmaceutics and New Drug Delivery Systems, Peking University, No. 38, Xueyuan Road, Beijing, 100191, People's Republic of China
[b] State Key Laboratory of Pharmaceutical Biotechnology, Nanjing University, Nanjing, 210023, Jiangsu, People's Republic of China

ARTICLE INFO

Keywords:
Gene therapy
Non-viral vector
Transdermal delivery
Gas6
Hair reproduction
Androgenetic alopecia

ABSTRACT

Androgenetic alopecia is an androgen-dependent skin disorder that commonly affects hair follicle growth and hair loss. Gene therapy that can promote the proliferation and survival of hair follicle cells can be a potential choice for its cure. While transdermal application of therapeutic functional nucleic acids across the stratum corneum is quite difficult. Here, we first develop a transdermal agent for functional nucleic acid delivery using Triton X-100-modified low molecular weight polyethyleneimine (PEI-Triton-N, N = 6 or 8). In vitro cell experiments demonstrate that the PEI-Triton-N conjugates can stably encapsulate and efficiently deliver plasmid DNA to hard-to-transfect keratinocyte HaCaT cells. Further mouse model studies show that PEI-Triton-6 can encapsulate and deliver growth arrest-specific protein 6 (Gas6) plasmid through transdermal administration. The transfected Gas6 prolongs the anagen status, inhibits the apoptosis of hair follicle cells, and further promotes the proliferation and differentiation of hair follicle cells. The PEI-Triton-6/$pDNA_{Gas6}$ complexes can obviously alleviate hair loss in androgenetic alopecia mice and provides a promising strategy for gene therapy via transdermal administration.

1. Introduction

Androgenetic alopecia, also known as seborrheic alopecia, is an androgen-dependent skin disorder that commonly affects young and middle-aged men with stagnant hair growth in the forehead area of the scalp. It is characterized by a progressive miniaturization of hair follicles and shortening of the hair growth period, resulting in a decrease in the number of hairs on the scalp and an increase in resting hair loss due to the transformation of hair follicles into vellus hairs [1]. Although androgenetic alopecia is not life-threatening, it has a significant negative impact on quality of life and mental health. The action mechanism of androgenetic alopecia is not yet fully known, the vast majority of studies suggest endocrine factors and genetic susceptibilities, such as androgen metabolism, inflammation of the hair follicle environment, age, patterns of life and diet influence the development cycle of hair follicles [2]. Normally, the restart of new growth in hair follicles is tightly regulated by niche signals to control cell behaviour and tissue homeostasis through specific cell-intrinsic molecular mechanisms. And dermal papilla fibroblasts, dermal adipose cells, immune cells, vascular cells, and nerve endings in the skin microenvironment were also involved in these signal regulations [3–6]. There are increasing evidences that dermal papilla cells also act as the organizing center to stimulate hair regeneration. Regulation of cytokines and growth factors from dermal papilla cells can improve hair growth in the treatment of alopecia [3,7]. Growth arrest-specific protein 6 (Gas6) is a soluble glycoprotein that was first identified in mouse embryonic fibroblasts and is involved in the stimulation of cell proliferation. After binding to its receptors (AXL, TYPO3 and MER), Gas6 activates tyrosine kinase activity and plays an important role in cell proliferation, survival, adhesion, migration, autophagy, invasion, angiogenesis, platelet aggregation and NK cell differentiation [8,9]. Restoring Gas6 protein in dermal papilla cells may reactivate the proliferation of hair follicle stem cells and is expected to reverse stress-induced hair loss, but its applicability to androgenetic alopecia remains to be verified [10].

Hair transplantation, stem cell therapy and small molecular drug treatments are still the mainstream treatment options for androgenetic alopecia. However, these treatments are costly, time-consuming and prone to conspicuous side effects such as impotence, irritation and dermatitis [11–13]. Recently functional nucleic acid drugs, such as plasmid DNA, mRNA, gRNA, siRNA and antisense oligonucleotide, have

* Corresponding author. State Key Laboratory of Natural and Biomimetic Drugs, School of Pharmaceutical Sciences and Chemical Biology Center, and Beijing Key Laboratory of Molecular Pharmaceutics and New Drug Delivery Systems, Peking University, No. 38, Xueyuan Road, Beijing, 100191, People's Republic of China.
E-mail address: xinjingt@pku.edu.cn (X. Tang).

https://doi.org/10.1016/j.mtbio.2023.100575
Received 16 December 2022; Received in revised form 16 January 2023; Accepted 1 February 2023
Available online 2 February 2023

gradually become hot spots in recent drug development [14]. Compared with the systemic administration of functional nucleic acid drugs, transdermal administration has limited systemic toxicity, avoiding quick excretion and liver accumulation. Generally, only small lipophilic molecules (<500 Da) can penetrate the skin at therapeutically adequate rates. However, the unique composition and structural organization of the skin make it difficult for hydrophilic nucleic acids to cross the stratum corneum and enter the deeper skin cells. This makes it an exceptionally challenging problem for the delivery of functional nucleic acids and the bottleneck of gene therapy for skin-related diseases [15].

There have now been a multitude of studies for the development of non-viral gene delivery vectors reported, typically comprising cationic lipids or cationic macromolecules, as formulation aids for nucleic acids. These nanoparticle systems have shown the possibility and efficiency as transdermal delivery systems for siRNA [16], mRNA [17], saRNA and pDNA [18]. Polyethyleneimine (PEI), a cationic polymer gene delivery vector with high cell transfection efficiency and lysosome escape ability, attracts much attention due to its advantages of flexible structure modification and low cost [19,20]. However, there was a positive correlation between high transfection efficiency and high toxicity. To tackle the internalization problem of functional nucleic acids, several modification strategies have been proposed [21–24]. Anionic polyacrylic acid (PAA) was electrostatically and covalently linked with PEI, which exhibited considerably higher pDNA transfection efficacy than the standard reagent lipofectamine [19]. A polyethyleneglycol-modified PEI--cholesterol lipopolymer that delivers IL-12 plasmid for the treatment of ovarian epithelial/fallopian tube cancer has completed phase II trials (NCT01118052). Delivery of functional nucleic acids has been achieved by modified PEIs in various cancer treatments, but there were few reports and applications of PEI in skin-related diseases.

Triton X-100, a nonionic surfactant with a hydrophobic head group and hydrophilic PEG terminal long chain, can maximize the natural conformation and function of cell membrane proteins, and significantly promote the permeability of eukaryotic cell membranes. In our previous work, Triton X-100 was used as an efficient transmembrane agent involved in an ATP-triggered siRNA delivery vector to improve the anticancer efficiency by intratumoral administration [25]. Here, we successfully developed a Triton X-100-modified PEI transfection vector for keratinocyte transfection and transdermal administration, in which Triton X-100 was used as an efficient neutral transmembrane reagent based on its traditional surfactant function to enhance in vitro and in vivo uptake of DNA plasmids. We used this vector to encapsulate the Gas6 plasmid for gene therapy on androgenetic alopecia mice and confirmed the promising application of the PEI-Triton-6/pDNA$_{Gas6}$ complexes for hair follicle development and growth, which is expected to provide a new strategy for gene therapy in skin-related diseases.

2. Materials and methods

2.1. Material

Low molecular weight polyethylenimine (branched, MW 1.8 kD) was purchased from Alfa Aesar (China). Triton X-100 was purchased from TCI (China). N, N′-disuccinimidyl carbonate was purchased from J&K (China). Testosterone propionate was purchased from Macklin. Phosphate-buffered saline, fetal bovine serum, Opti-MEM, and trypsin were purchased from Macgene (China). Hoechst 33342 and LysoTracker Deep Red were purchased from Thermo Fisher Scientific Inc. (USA). 3-(4,5-Dimethylthiazol-2-yl)2,5-diphenyltetrazolium bromide (MTT) and carboxymethylcellulose sodium (Mw 90 k) were purchased from Solarbio (China). pEGFP-N1, pcDNA3.1-mCherry were purchased from Fenghuibio Co. Ltd and propagated in competent *Escherichia coli* DH5α cells (Solarbio, China). Amplified mGas6 consequences (NM_019521.2) were cloned into the pcDNA3.1-mCherry backbone through double digestion. 5% minoxidil gel was purchased from Bausch & Lomb Freida (China).

2.2. Cell lines and animals

HaCaT cells, HEK-293T, MCF-7 and HeLa cells were all provided by the National Infrastructure of Cell Line Resource. All cell lines were cultured within the Dulbecco's Modified Eagle Medium (DMEM) complete medium that contained 10% fetal bovine (FBS) medium and 1% penicillin-streptomycin. All cell lines were cultivated at 37 °C in a 5% CO_2 atmosphere. All animal experiments were approved by the Peking University Experimental Animal Welfare Ethics Review Committee.

2.3. Synthesis of PEI-Triton-N conjugates

A solution of Triton X-100 (150 mg, 0.23 mmol) and triethylamine (97 μL, 0.70 mmol) in dichloromethane (2.5 mL) was added dropwise to N, N′-disuccinimidyl carbonate (90 mg, 0.35 mmol), and the mixture was stirred at room temperature overnight. Then the solution was washed with ddH_2O three times, and the organic phase was dried. After evaporation, the obtained yellow oil residue was directly used for the next step reaction without further purification. The solution of the above Triton X-100-NHS was added to PEI 1.8 kDa in dichloromethane. The mixture was stirred at room temperature for 24 h. The solution was concentrated and the residue was then dissolved in distilled water and purified by dialysis against 30% methanol solution for 24 h with six times solution exchanges. The dialysate was lyophilized to obtain the final product. PEI 1.8 kDa labeled with different amounts of Triton X-100 were achieved by adjusting the equivalent ratios of two reactants and characterized using ^{1}HNMR. The as-prepared conjugates were named PEI-Triton-N (N = 4, 6, 8).

2.4. Formation and characterization of PEI-Triton-N/pDNA

PEI-Triton-N/pDNA complexes were prepared by mixing plasmid DNA (pDNA) stock solution with various amounts of PEI-Triton-N conjugates. Briefly, the PEI-Triton-N solution was added to pDNA stock solution, followed by 10 s vertexing and another 15 min incubation at room temperature. The ratio of PEI-Triton-N/pDNA was calculated as the nitrogen/phosphate (N/P) ratio. PEI 1.8 kDa/pDNA complexes were similarly prepared as a control.

The DNA encapsulation ability of PEI-Triton-N/pDNA was assessed with agarose gel electrophoresis. Briefly, PEI-Triton-N/pDNA complexes with different N/P ratios (containing a fixed amount of 200 ng pDNA) were prepared with a final volume of 10 μL. The samples were run with 2% agarose gel for 15 min in tris-acetate buffer and the gels were developed using a ChemiDoc XRS gel imaging system. To investigate the effect of Triton X-100 modification on the release efficiency of DNA from the PEI-Triton-N/pDNA complexes, heparin sodium was used to competitively replace the DNA in the complex. PEI-Triton-N/pDNA complexes with an N/P ratio of 7 were prepared, and then different amounts of heparin (heparin/pDNA mass ratio from 0 to 10) were added to the complexes solution. The samples were incubated at 37 °C for 30 min, followed by agarose electrophoresis. At the same time, PEI 1.8 kDa/pDNA and PEI 25 kDa/pDNA were prepared as controls.

The serum and DNase stability of PEI-Triton-N/pDNA complexes were determined by agarose gel electrophoresis. PEI-Triton-N/pDNA complexes with an N/P ratio of 7 were prepared, and 10% serum or DNase I (6 U/μg pDNA) was then added to the complexes solution for further incubation from 0.5 h to 36 h. Naked plasmid DNA was used as a control under the same conditions. The agarose gels were imaged as mentioned above.

The particle sizes and ζ-potentials of the PEI-Triton-N/pDNA complexes were measured using a Malvern Zetasizer Nano. The morphology of PEI-Triton-N/pDNA complexes was characterized by scanning electron microscopy. Then, 20 μL PEI-Triton-N/pDNA complex solution (N/P 30) was dropped onto a 100-curved silicon wafer. The solution was evenly dispersed on a silicon wafer and dried naturally.

2.5. Cytotoxicity analysis

The cytotoxicity of PEI-Triton-N conjugates against HaCaT cells was determined using a 3-(4,5-dimethylthiazol-2-yl)2,5-diphenyltetrazolium bromide (MTT) assay. Briefly, cells were counted and plated in 100 μL media at 8×10^3 cells per well in 96-well plates. After 24 h, the cells were treated with various concentrations of PEI-Triton-N conjugates for 48 h. Then, MTT reagent was added to 20 μL of each well. The cells were incubated with MTT for 4 h at 37 °C, followed by a replacement with DMSO to dissolve the formazan. Then, the absorbance of each well at 490 nm was analyzed with a FlexStation 3 Benchtop MultiMode Microplate Reader.

2.6. In vitro plasmid DNA transfection and expression

For the in vitro transfection experiment, HaCaT cells were seeded at a density of 1×10^5 cells per well and cultured for 24 h. Then, the cells were treated with the complexes of PEI-Triton-6 or PEI-Triton-8 with EGFP plasmid at various N/P ratios in an Opti-MEM medium for 4 h. After replacement with fresh complete growth media, the cells were incubated for an additional 48 h. Then, EGFP expression was observed and quantitatively analyzed by fluorescence microscopy and flow cytometry. Cells transfected with PEI 25 kDa/$pDNA_{EGFP}$ and lipofectamine/$pDNA_{EGFP}$ complexes were used as the control group according to the above protocol. Meanwhile, HEK-293T cells, HeLa cells and MCF-7 cells were also chosen to evaluate the transfection efficiency of PEI-Triton-N/pDNA complexes separately. All experiments were performed in triplicates.

2.7. Intracellular trafficking of PEI-Triton-N/pDNA

The cellular uptake of PEI-Triton-N/pDNA complexes was also evaluated with confocal laser scanning microscopy. For the observation of endo/lysosomal escape, HaCaT cells were seeded into 35 mm confocal glass-bottom culture dishes and cultured for 24 h. Then, the cells were treated with TRITC modified PEI 25kD/pDNA and PEI-Triton-N/pDNA complexes at various N/P ratios in Opti-MEM medium without FBS for 4 h. After replacement with fresh complete growth media, the cells were incubated for an additional 3 h, 6 h, and 8 h. The cells were then washed and stained with Hoechst 33342 and Lyso Tracker solution for 30 min at 37 °C. The cells were finally imaged using confocal laser scanning microscopy (LSM 880, Carl Zeiss).

2.8. Transdermal delivery of mCherry DNA plasmid with PEI-Triton-N/$pDNA_{mCherry}$

Six-week-old C57BL/6 male mice were randomly divided into three groups. The dorsal hair of all mice was removed under 4% chloral hydrate anesthesia. PEI-Triton-6/$pDNA_{mCherry}$ (N/P 40), PEI-Triton-8/$pDNA_{mCherry}$ (N/P 40) and PEI25KDa/$pDNA_{mCherry}$ (N/P 20) complexes containing 60 μg mCherry plasmids were prepared. The above solutions were allowed to respectively incubate with the exposed skin for 6 h while keeping animals under minimal anesthesia and once per day for 7 days before animals were sacrificed. Skin biopsies were collected from the treated area of the animal skin and then immediately frozen in OCT compound and sectioned at a thickness of 20 μm on a freezing microtome (M3050, Leica). All sections were imaged using CLSM at 561 nm/610 nm to examine the expression of the fluorescent protein mCherry in mouse skin.

2.9. AGA-induced mouse model and skin administration of PEI-Triton-6/$pDNA_{Gas6}$ gel complexes

Testosterone propionate solution in corn oil was applied to dorsal skin daily (5 mg/kg, s. c.) for 28 days in 6-week-old C57BL/6 male mice to generate an androgenetic alopecia model. Normal control mice were treated with corn oil without testosterone propionate. PEI-Triton-6/$pDNA_{Gas6}$ complexes were prepared in the same way as cell experimental method. Then, carboxymethylcellulose sodium (CMC) was ground with glycerol evenly, and an appropriate amount of distilled water was gradually added to swell as a hydrogel matrix. Finally, the CMC hydrogel matrix was stirringly mixed with PEI-Triton-6/$pDNA_{GAS6}$ solution to form PEI-Triton-6/$pDNA_{GAS6}$ gel complexes. (The pDNA-loaded complexes were dissolved in 1 mL of distilled water which contained 40 μg pDNA and 260 μg/mL PEI-Triton-6.) The ratio of CMC was determined at 3.25% and glycerol as a moisturizer at 6.5% (v/v). Dorsal hair of mice was completely removed before topical administration and mice were randomly divided into four different treatment groups, including normal control mice (Ctrl, n = 5), androgenetic alopecia control mice (AGA/Ctrl, n = 7), androgenetic alopecia mice treated with PEI-Triton-6 complexes containing 40 μg pcDNA3.1-Gas6-mcherry plasmid (AGA/Gas6, n = 5), and androgenetic alopecia mice treated with 5% minoxidil gel (AGA/Minoxidil, n = 5) as the positive group. Mice in each group were applied with different treatments on the back daily under non-anesthetic conditions. Body weights and hair growth statuses were recorded and photographs were taken daily. Dorsal hair growth was evaluated by assessing skin color and hair density. Mice were anesthetized with 2.5% avertin and sacrificed after 26 days of treatment via topical administration. Dorsal hair from the same size of skin area for each group was redepilated and was then weighed using a precision balance. Dorsal skin tissues were collected for histopathology and biochemical assays.

2.10. Androgen levels in serum

Blood samples were harvested on Day 26 from the postocular venous plex on mice under anesthesia. For serum, the whole blood was collected and clotted at 4 °C overnight and then centrifuged at 3000 rpm to separate the supernatant. The androgen level in the serum was analyzed by ELISA kits (Yojanbio).

2.11. Histological and immunofluorescence staining

Dorsal skin samples were fixed in 4% paraformaldehyde for paraffin slices and 30% sucrose solution for frozen slices. Longitudinal sections of hair follicles were prepared and stained with hematoxylin and eosin. Hair follicle proliferation and regression were analyzed through Ki67 immunohistochemistry (1:50 dilution, CST) and TUNEL staining. Images were obtained and analyzed using a digital pathology slice scanner (zhiyue) and Vectra Polaris (PE).

2.12. Quantitative RT-PCR and western blot analysis

Dorsal skin samples were frozen and ground to powder in liquid nitrogen. Total RNA was extracted using TRIzol® reagent according to the manufacturer's protocol, and first-strand cDNAs were reverse-transcribed with the GoScript™ Reverse Transcription System (A5001) (Promega). All real-time PCRs were performed with the SYBR Mix kit (Promega) using an ABI Q6 Real-Time system. Target gene mRNA levels were normalized to β-actin mRNA levels. The primers used were as follows: Gas6: 5′- CCGCGCCTACCAAGTCTTC-3′(forward) and 5′-CGGGGTCGTTCTCGAACAC-3′(reverse); β-actin: 5′- GTGACGTTGACATCCGTAAAGA-3′(forward) and 5′- GCCGGACTCATCGTACTCC-3′(reverse). Relative gene expression was calculated by using the $2^{-\Delta Ct}$ method. Total proteins were gathered in RIPA buffer with a proteinase inhibitor cocktail and phosphatase inhibitor. The primary antibodies used for western blot analysis were anti-Gas6 (1:500 dilution, Solarbio), anti-Bcl-2 (1:500 dilution, Applygen), anti-Stat3 (1:500 dilution; Abcam), anti-phospho-Stat3 (Tyr705) (1:500 dilution; Affinity), and anti-β-actin (1:1000 dilution; Abcam). Analysis of the grayscale intensity of the protein band density was proceeded using ImageJ analysis software and normalized to the grayscale of β-actin.

2.13. Data analysis

All the experiments in this paper were repeated more than three times. The significant difference analysis and P value were calculated by Mean ± SEM expression, analyzed by Student's t-tests and two-way ANOVA test. $P < 0.05$ (*) was considered a statistically significant difference, $P < 0.01$ (**) represents a very significant difference, and $P < 0.001$ (***) represents an extremely significant difference.

3. Results and discussion

3.1. Synthesis and characterization of pDNA-loaded PEI-Triton-N complexes

Triton X-100-modified PEI (PEI-Triton-N) was synthesized as shown in Fig. 1. The hydroxyl group of Triton X-100 reacted with N, N′-disuccinimidyl carbonate to form its NHS ester, which further reacted with the primary amine group of PEIs. Triton X-100 modified PEI conjugates at different equivalent Triton/PEI ratios were obtained. The conjugates were purified by dialysis in a 30% methanol aqueous solution for 24 h to remove unreacted PEI 1.8 kDa and Triton X-100, and these residues were further lyophilized for subsequent use. The number of Triton X-100 per PEI was confirmed using ^{1}HNMR, named PEI-Triton-N. As shown in Fig. S1, the peaks occurring at δ 6.86–6.82 ppm were ascribed to the phenyl proton signals of Triton X-100, and the peaks appearing at δ 3.3–2.4 ppm belonged to the amine proton signals of PEI 1.8 kDa. Finally, three PEI-Triton-N conjugates (PEI-Triton-4, PEI-Triton-6, PEI-Triton-8) were obtained for the following evaluation.

The DNA binding ability of PEI-Triton-N conjugates was investigated by agarose gel electrophoresis at different N/P ratios (vectors/DNA) from 0 to 7. As shown in Fig. 2A, PEI 25 kDa and PEI 1.8 kDa could efficiently encapsulate pDNA at N/P ratios of 0.5 and 2 respectively, while PEI-Triton-6 and PEI-Triton-8 completely inhibited DNA migration at lightly higher N/P ratios of 4 and 5. It was due to a little bit lower density of the positive charge for PEI-Triton-N conjugates. The PEI-Triton-6/pDNA complexes began to dissociate at a relatively low heparin/pDNA ratio of 2, and the PEI-Triton-8/DNA complexes dissociated at a heparin/pDNA ratio of 1, while pDNA released from the PEI 1.8 kDa/pDNA complexes needed a much higher ratio of heparin/pDNA (ratio of 6) as shown in Fig. 2B. This phenomenon demonstrated that pDNA more easily dissociated from the PEI-Triton-N/pDNA complexes in comparison to the PEI 1.8 kDa/pDNA complexes due to the milder electrostatic interaction between Triton X-100-modified PEI and pDNA. For the stability of encapsulated pDNA in PEI-Triton-N complexes, DNase and serum were then applied. For the DNase stability assay, the PEI-Triton-6/pDNA complex was incubated with 6U DNase I/ug pDNA, and the samples were allotted at different time intervals. As shown in Fig. 2C, the DNA band of PEI-Triton-6/pDNA was not obviously degraded up to 12 h, while the naked pDNA was immediately degraded by DNase I within 2 h under the same assay. A similar observation was also found in serum incubation. When naked pDNA and PEI-Triton-6/pDNA complex were incubated with 10% serum, the pDNA stability of PEI-Triton-6/pDNA complex was greatly enhanced and remained stable after 36 h incubation, while the band of naked DNA gradually decreased and almost fully disappeared after 12 h. Both serum stability and DNase stability assay results confirmed that the condensed DNA was protected by Triton X-100-modified PEI conjugate, indicating its promising applications for cellular and transdermal administration. The particle size and surface charge of PEI-Triton-N/pDNA complexes had significant effects on cellular uptake and distribution of the complexes, as well as cellular cytotoxicity and tissue compatibility. As shown in Table S1, with the increase of the N/P ratios, the size and ζ-potential of the PEI-Triton-N/pDNA nanocomplexes also increased. PEI-Triton-6/pDNA complexes were stable in H_2O solution and 10% FBS, and their particle sizes were consistent as shown in Fig. S2. In addition, SEM images (Fig. 2D) showed that PEI-Triton-6 and PEI-Triton-8 could encapsulate plasmid DNA into

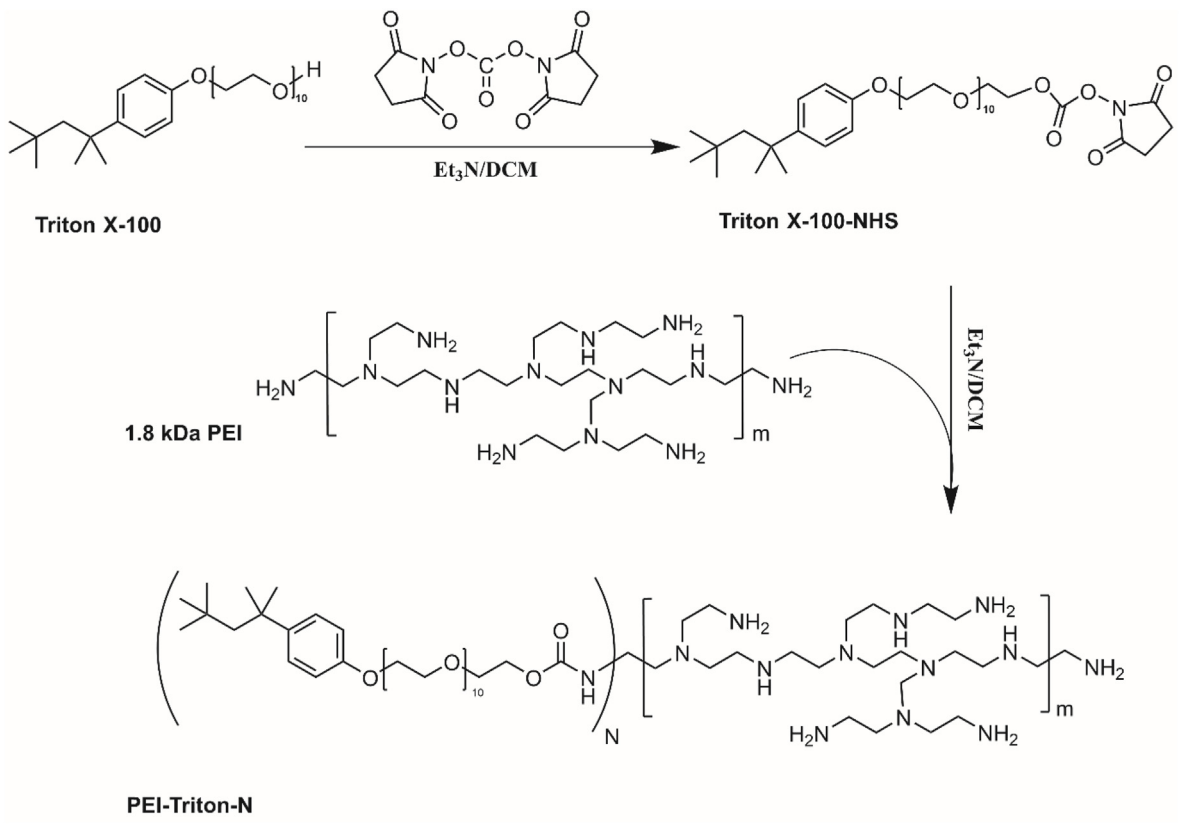

Fig. 1. Schematic illustration of synthetic PEI-Triton-N conjugates.

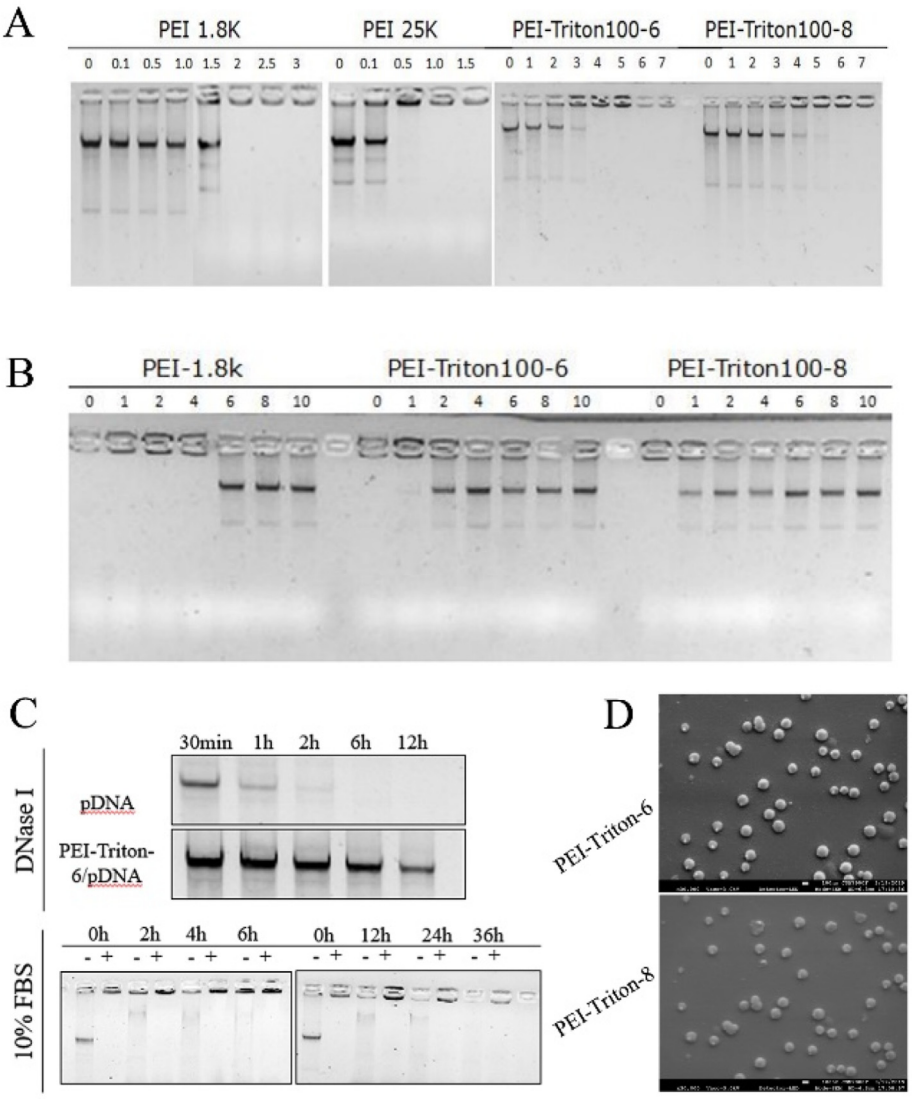

Fig. 2. Characterization of PEI-Triton-N/pDNA complexes. (A) Agarose gel electrophoresis of DNA encapsulation ability. (B) Agarose gel electrophoresis of DNA release ability. (C) Agarose gel electrophoresis of 10% serum and DNase I stability. (D) Scanning electron microscope images of plasmid-loaded PEI-Triton-6 and PEI-Triton-8 complexes.

spherical nanoparticles approximately 200 nm in diameter at an N/P ratio of 30, which were smaller than those measured in the hydrated solution (358.2 ± 3.2 nm and 326.0 ± 17.5 nm). These results might be ascribed to particle hydration and PEG modification of PEI-Triton-N moieties.

3.2. Cytotoxicity assay in vitro

Further characterization of PEI-Triton-N conjugates was evaluated in hard-to-transfect keratinocyte HaCaT cells. The cytotoxicity of PEI-Triton-N conjugates was first evaluated in HaCaT cells. As shown in Fig. S3, the higher positive charge density of PEI 25 kDa showed obvious cytotoxicity, while PEI 1.8 kDa showed little toxicity on normal cell proliferation due to the low molecular weight as expected. Similarly, the cytotoxicity of PEI-Triton-6 and PEI-Triton-8 was also much lower in comparison to that of PEI 25 kDa, and the cell viability was still up to 90% at the concentration of 10 μg/mL PEI-Triton-N conjugates.

3.3. Cellular uptake and intracellular trafficking in vitro

The cellular uptake and transfection efficiency of PEI-Triton-N/$pDNA_{EGFP}$ complexes were performed on HaCaT cells based on the expression level of EGFP using flow cytometry and CLSM. Lipofectamine/$pDNA_{EGFP}$ and PEI 25 kDa/$pDNA_{EGFP}$ complexes were also prepared with N/P ratios of 20 as a control (a high N/P ratio for PEI 25 kDa caused the obvious cell death). As shown in Fig. 3, EGFP fluorescence in cells treated with the PEI 25 kDa/$pDNA_{EGFP}$ group was very low, while cells treated with the PEI-Triton-6/$pDNA_{EGFP}$ and PEI-Triton-8/$pDNA_{EGFP}$ complexes showed significant enhancement of the EGFP signal with the increase of N/P ratios from 10 to 40. In particular, when the N/P ratio reached up to 40, the EGFP fluorescence expression of PEI-Triton-6/$pDNA_{EGFP}$ and PEI-Triton-8/$pDNA_{EGFP}$ was approximately 1.5 and 2.0-fold higher than that of the Lipofectamine/$pDNA_{EGFP}$ group, respectively. As also shown in Fig. S4, the proportion of EGFP (+) cells in PEI 25 kDa and lipofectamine treated group are 1.78% ± 0.99% and 23.79% ± 2.98%, which were significantly lower than those of PEI-Triton-6 (38.05% ± 3.98%) and PEI-Triton-8 (47.10% ± 3.00%). The transfection efficiency of PEI-Triton-N in three other cell lines (HEK 293T, HeLa and MCF-7) were also evaluated, as shown in Figs. S5–S7. The EGFP expression of PEI-Triton-6/$pDNA_{EGFP}$ in HEK 293T, HeLa and MCF-7 cells was also approximately 1.8, 1.8 and 1.5-fold higher than that in the Lipofectamine/$pDNA_{EGFP}$ treated group, and PEI-Triton-6 had the most stable and highest plasmid

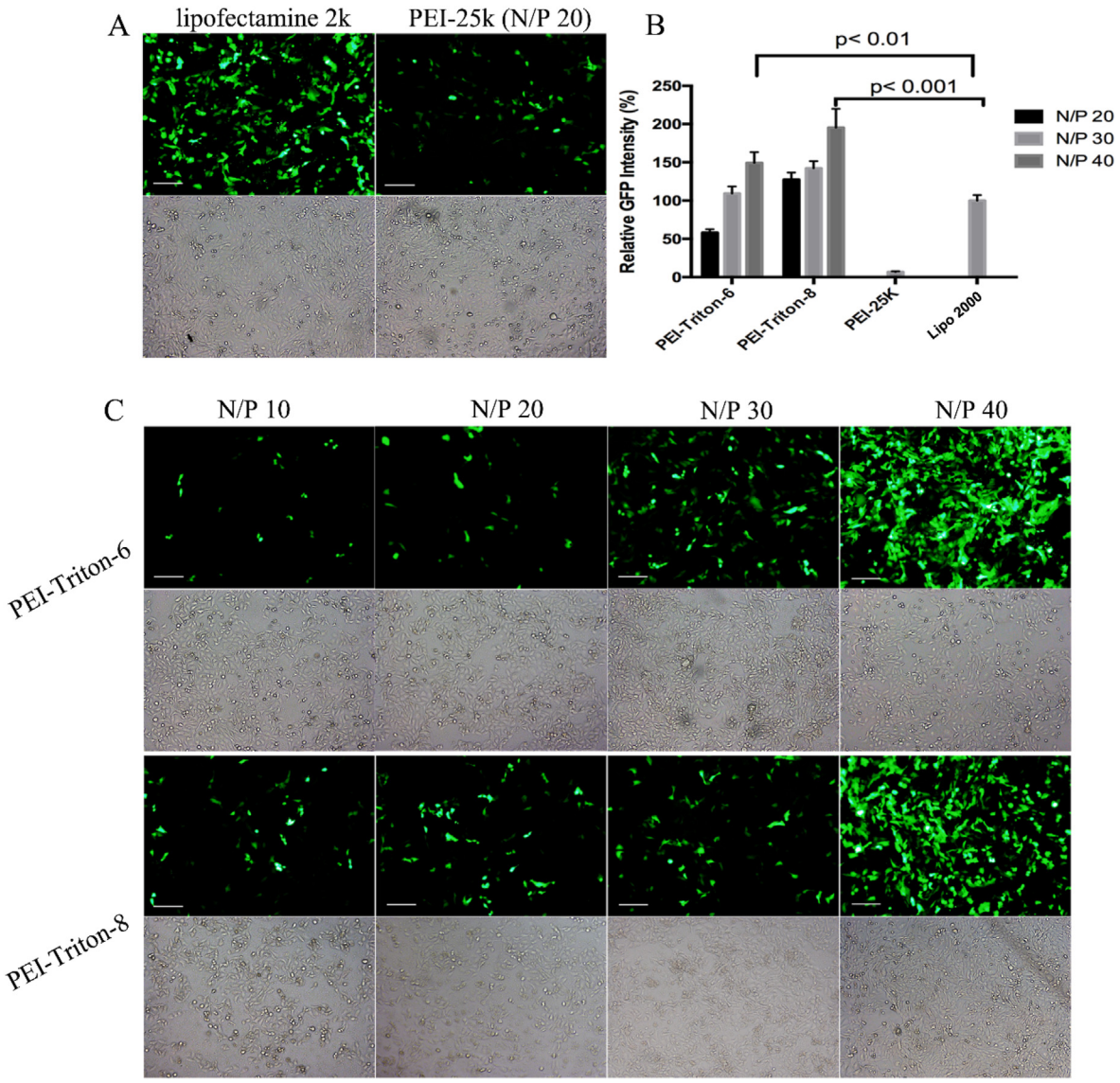

Fig. 3. The expression of EGFP fluorescence protein after treatment with PEI-Triton-N/pDNA$_{EGFP}$ complexes at different N/P ratios in HaCaT cells, which was performed by fluorescence imaging, brightfield (A, C) and flow cytometry (B). Scale bar = 500 μm. Data are shown as mean ± SEM (n = 3; two-way ANOVA test; *p < 0.05; **p < 0.01; ***p < 0.001).

transfection efficiency in these kinds of cells.

Further time-dependent co-localization experiments were also investigated (Fig. 4). After the TRITC modified PEI-Triton-6/pDNA complexes were incubated with HaCaT cell for 3 h, we observed the trapping of PEI-Triton-6/pDNA complexes in endosome/lysosome with the overlapping fluorescence signals of TRITC (green) and Lyso Tracker Red (Pearson constant 0.92). However, TRITC green signals were separated from the red signals of Lyso Tracker Red after 6 h (Pearson constant 0.59). After approximately 8 h of incubation, the TRITC signal of PEI-Triton-6/pDNA complexes was obviously isolated with a red signal of LysoTracker Red in endosome/lysosome with Pearson constant less than 0.3. These results indicated that TRITC-PEI-Triton-6/pDNA complexes successfully escaped from the endosome/lysosome, which was a vital process for plasmid delivery and further gene function. This result was probably due to the excellent transmembrane effect of Triton X-100 and the "sponge effect" of PEI 1.8 kDa in the Triton-PEI conjugate, which successfully promoted endosome/lysosome escape and DNA plasmid release. As the control PEI 25kD group shown in Fig. S8, the cellular uptake ability of TRITC-modified PEI 25 k/pDNA in HaCaT cells was very low, and consistent with the EGFP (+) cells rate only reaching 1.78% ± 0.99% in Fig. S4.

3.4. Skin penetration of PEI-Triton-N conjugates in vivo

The high skin penetration ability of PEI-Triton-N in vivo was further investigated as shown in Fig. S9. To analyze the transfection efficiency of plasmid DNA using PEI-Triton-N delivery agents, PEI 25 kDa/pDNA$_{mCherry}$, PEI-Triton-6/pDNA$_{mCherry}$ and PEI-Triton-8/pDNA$_{mCherry}$ complexes were performed on intact mouse skin. Then, frozen sections of skin tissue slices were prepared and analyzed by fluorescence microscopy. Upon transfection with PEI-Triton-6/pDNA$_{mCherry}$ complexes, the expression of mCherry protein was obviously higher than that of PEI 25 kDa/pDNA$_{mCherry}$ groups. Deep penetration and homogeneous expression of mCherry protein into the dermis were obviously observed in the PEI-Triton-6 treatment group in comparison to the control group.

3.5. Hair regrowth effects of PEI-Triton-6/pDNA$_{Gas6}$ in AGA-induced mice

Based on the above skin permeability efficiency of PEI-Triton-6/pDNA complexes, we investigated the effect of Gas6 plasmid on hair growth and hair follicle development in androgenetic alopecia mice using PEI-Triton-6 delivery reagent. Topical application of 5% minoxidil

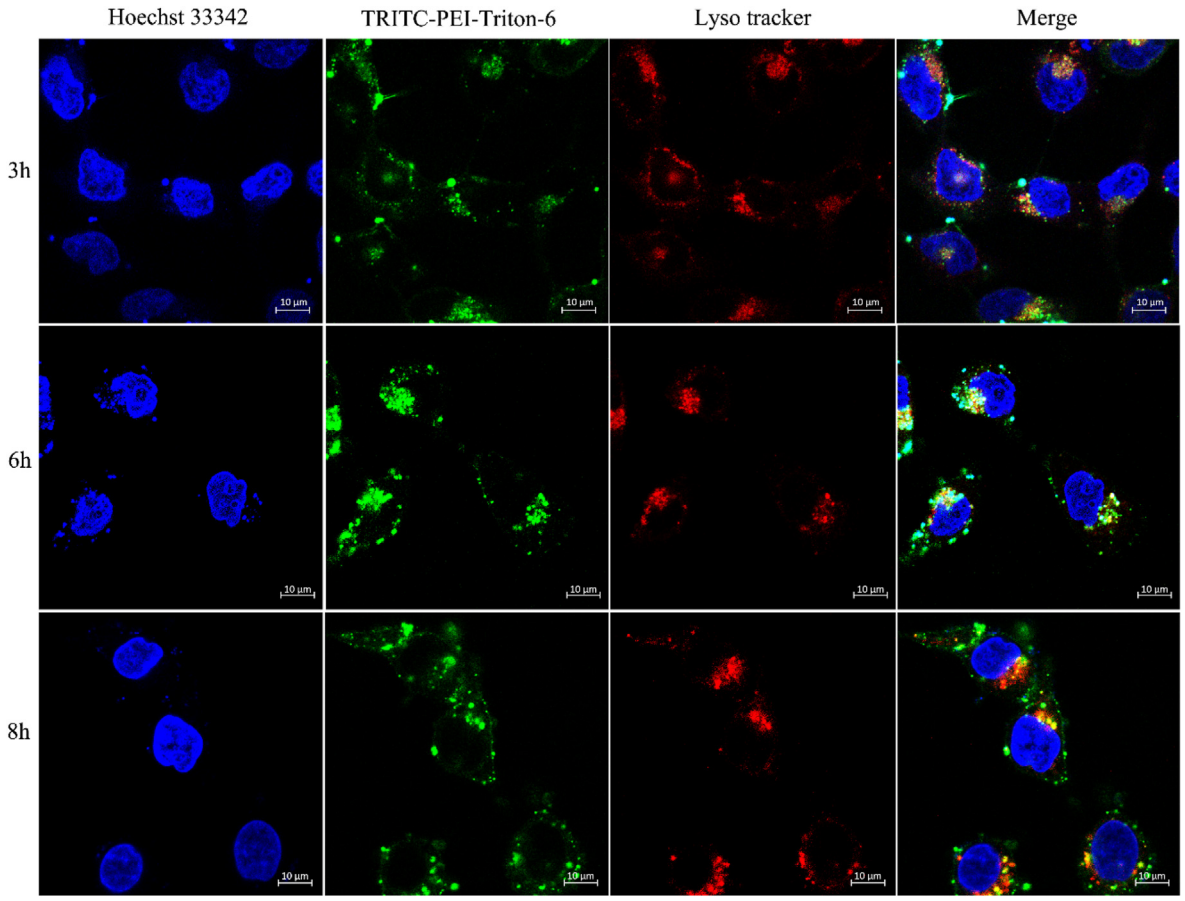

Fig. 4. Intracellular trafficking of TRITC-PEI-Triton-6/pDNA complexes in HaCaT cells. PEI-Triton-6 was labeled with TRITC (Green channel), and nuclei and endo/lysosomes were stained with Hoechst 33342 (Blue channel) and Lyso Tracker DeepRed (Red channel), which were imaged by confocal laser microscopy. Scale bar = 10 μm. (For interpretation of the references to colour in this figure legend, the reader is referred to the Web version of this article.)

gel was used as a positive control, and PEI-Triton-6/pDNA$_{Gas6}$ gel complexes were prepared for convenient skin administration according to references. [26,27] Testosterone propionate was subcutaneously injected into the dorsal skin of C57BL/6 mice for 28 days to establish a human androgenetic alopecia-like hair loss mouse model with elevated serum androgen expression levels (Fig. S10). The melanogenic activity of the hair follicle is closely related to the hair growth cycle, and the skin color gradually changes from pink to dark grey with the accumulation of melanin. For normal mice, hair follicles on the dorsal skin of the depilated mice were stimulated to enter a new anagen for about 13 days. With the gradual apoptosis of melanocytes and hair follicles entering the catagen period, the skin appeared grayish white for 6 days. Then, hair follicles eventually entered the telogen period with pink skin. However, the anagen phase of hair follicles was shortened and prematurely entered catagen with miniaturized hair follicles, causing hair loss in androgenetic alopecia mice. As shown in Fig. 5, on the first day of shaving dorsal skin, the dorsal skin of all mice appeared pink. After the 9th day of continuous topical administration, the skin gradually turned grey and entered into early-anagen, including the normal control, AGA/Minoxidil positive group and AGA/Gas6 treatment group. After the 14th day of topical administration, the AGA/Minoxidil and AGA/Gas6 treatment groups were performed in the rapid hair growth stage, but only a few areas of AGA/Ctrl treated hair follicles entered the early-anagen stage. On the 20th day of topical administration, the normal control group had dense hair and greyish white skin on catagen status, and the AGA/Ctrl model group had a large area of bare skin, while the AGA/Gas6 and AGA/Minoxidil treatment groups were completely covered with dorsal hair and black skin. Until the end of the experiment on Day 26, the hair of the AGA/Ctrl group was still short and thin, but the AGA/Gas6 treatment group was similar to the normal control and AGA/Minoxidil groups, which significantly alleviated the symptoms of androgenetic alopecia in mice.

Considering the systemic effects of percutaneous absorption with PEI-Triton-6, tetramethylrhodamine (TRITC) labeled PEI-Triton-6/pDNA$_{GAS6}$ gel complexes was applied on intact mouse skin daily. As shown in Fig. S11, there was no obvious fluorescence accumulation in other organs and blood except skin tissue. During the transdermal administration, no redness, ulceration or allergy was found in the skin of AGA/Gas treated mice. At the end of the 26-day treatment in vivo experiment, we took the skin tissue at the administration site for H&E staining (shown in Fig. S12). The connective tissue in the dermis of the AGA/Ctrl group was reduced, leading to atrophy of the dermis and a decrease in the number of hair follicles. The cortical structure of the AGA/Gas6 administration group was consistent with that of the normal control and positive AGA/Minoxidil group. The epidermis, dermis and subcutaneous in those groups were intact. Hair follicle morphology was normal and no obvious inflammatory reaction was observed. H&E staining of other organs also showed that the tissues from all administrated mice maintained typical normal histophysiology, confirming the safety of PEI-Triton-6/pDNA complex for topical administration instead of systemic absorption and toxicity. In addition, CMC and glycerol in the preparation of PEI-Triton-6/pDNA$_{GAS6}$ gel complexes greatly improved the ease of manipulation and good animal compliance during the treatment of androgen alopecia. As a commonly inactive excipient approved by FDA in topical administration gels, CMC does not affect hair follicle growth and development [28].

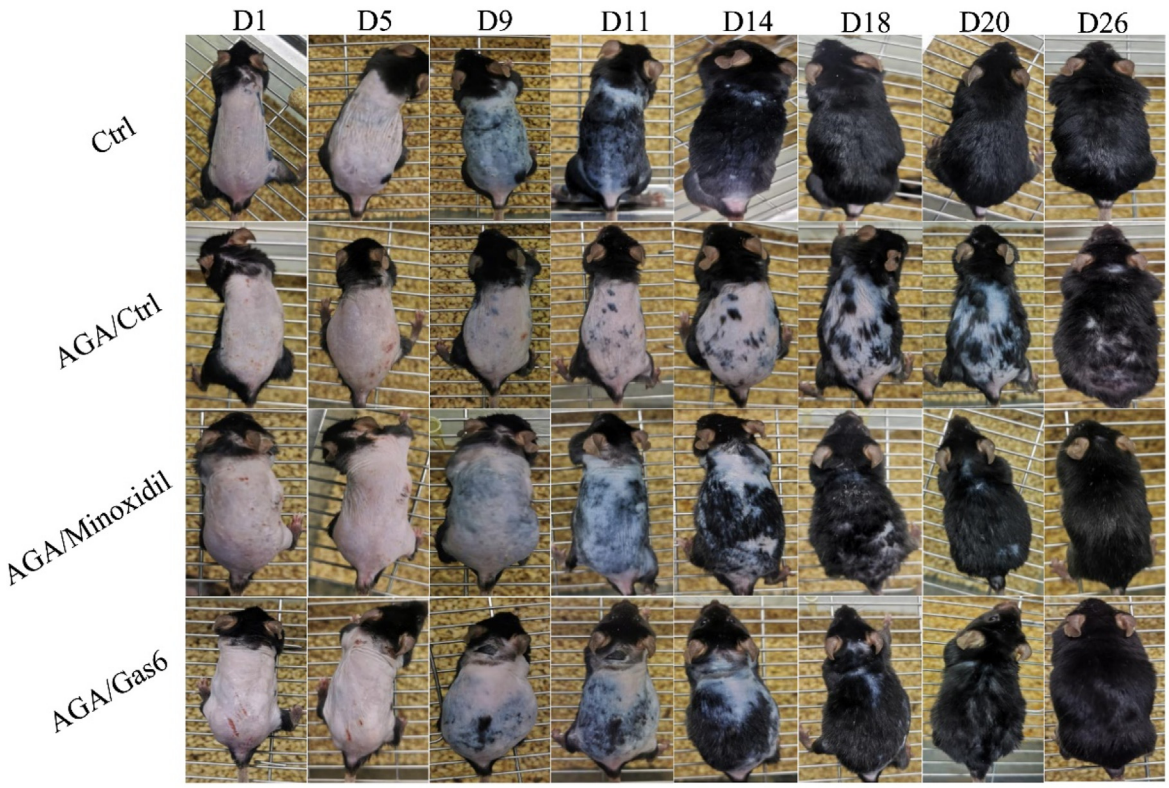

Fig. 5. Changes in dorsal skin and hair growth on normal mice (Ctrl) and androgenetic alopecia mice after treatment with negative control (AGA/Ctrl), 5% minoxidil gel (AGA/Minoxidil) and PEI-Triton-6/pDNA$_{Gas6}$ complexes (AGA/Gas6) for 26 days.

3.6. Histopathology and molecular evaluations of PEI-Triton-6/pDNA$_{Gas6}$ complexes treated AGA-induced mice

Hair regrowth of the androgenetic alopecia mice was first recorded and evaluated by the skin color assessment scale (Fig. 6A). The dorsal hair from the same area was shaved and weighed with a precision balance. As shown in Fig. 6B and **C**, the AGA/Gas6 group significantly prolonged hair follicle anagen. The density of hair regrowth was comparable to that of the normal controls and significantly higher than that of the AGA/Ctrl model group. To investigate the effect of Gas6 on hair follicle development, dorsal skin samples from normal mice and androgenetic alopecia mice with transdermal administration were collected and performed on histopathological and molecular level analysis. To observe the transdermal delivery efficiency of the PEI-Triton-6/pDNA$_{Gas6}$ complexes, frozen sections of dorsal skin tissue were prepared and imaged with a fluorescence microscope. Fluorescent imaging data (Fig. 6D) showed that the pcDNA3.1-Gas6-mCherry plasmid was successfully delivered into the dermis and the corresponding mCherry protein was highly expressed around hair follicles after transdermal administration of the PEI-Triton-6/pDNA$_{Gas6}$ complexes. As shown in Fig. 6E, H&E staining of paraffin sections indicated that the hair follicles in the AGA/Ctrl group showed miniaturized atrophy and the number of hair follicles was reduced significantly in the field of view. The visual field was mostly vellus hair follicles with mild pigmentation, where the diameter was shorter than the inner root sheath (shown by green arrows). It was a typical pathological change of androgenetic alopecia. However, few vellus hair follicles were observed in the AGA/Gas6 treatment group, which was similar to that of the normal control group. After 26 days of continuous topical administration, AGA/Gas6 treated mice had more terminal hair follicles with darker pigmentation and larger diameters (shown by red arrows), indicating that Gas6 affected hair follicle growth and development. It was reported that Gas6 could promote the proliferation of mesangial cells via signal transducer and activator of transcription 3 (STAT3) [29]. STAT3 was found to directly associate with the Bcl-2 gene promoter and upregulate Bcl-2 expression, thereby suppressing apoptosis [30]. Therefore, we further verified the expression of proliferation and apoptosis in skin tissue sections. As shown in Fig. 6F, immunofluorescence staining with the apoptosis marker TUNEL showed that the number of TUNEL (+) cells in the AGA/Gas6 group were lower than that of the AGA/Ctrl group. Immunohistochemical staining of skin sections showed that the numbers of Ki67 (+) cells, a proliferation marker, in the AGA/Gas6 group were also higher than those in the AGA/Ctrl group and were comparable to those in the normal control group. To further confirm the modulation of Gas6 expression at the mRNA level, real-time PCR of Gas6 mRNA was carried out with β-actin mRNA as the internal control. As shown in Fig. 6G, Gas6 mRNA transcription in the AGA/Gas6 treatment group was 2.5-fold higher than that in the other groups at the topical administration site. However, the Gas6 expression in mice skin outside the topical administration site was low and had no difference in comparison to the control group (Fig. S13). In addition, total proteins were further extracted from skin tissues in each treatment group. Gas6 and apoptosis-related proteins were then specifically analyzed by western blotting. As shown in Fig. 6H–K, the expression of the Gas6 protein in the AGA/Gas6 treatment group was significantly higher than in normal control and AGA/Ctrl groups. The expression level of phosphorylated STAT3 in the AGA/Gas6 treatment group was nearly twice as high as those in the normal mice group and AGA/Ctrl group. Meanwhile, the expression level of the antiapoptotic protein Bcl-2 in the AGA/Ctrl was only half of that in the normal mice, which was consistent with the damaged phenotype and TUNEL results of hair follicles. Testosterone propionate affected the normal development of hair follicles and promoted their apoptosis. However, after continuous transdermal administration of PEI-Triton-6/pDNA$_{Gas6}$, the expression level of Bcl-2 was significantly upregulated with a three-fold enhancement in comparison to that of the AGA/Ctrl group. Therefore, we clarified that the upregulation of Gas6 protein expression in the AGA/Gas6

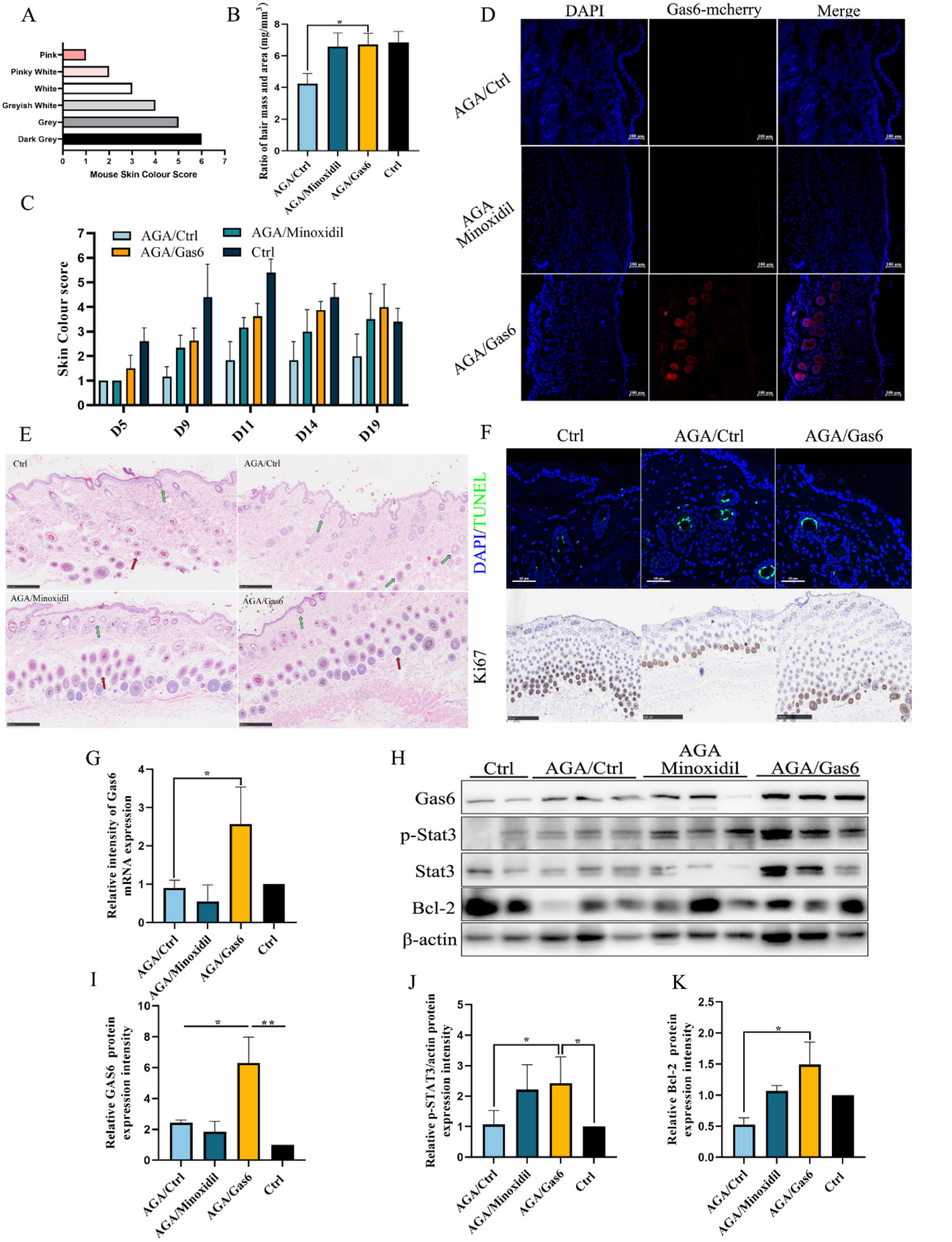

(caption on next page)

Fig. 6. The therapeutic effect of PEI-Triton-6/GAS6 complexes on hair growth and hair follicle development in androgenetic alopecia mice via transdermal administration, including normal control mice (Ctrl), androgenetic alopecia control mice (AGA/Ctrl), PEI-Triton-6/Gas6 treated androgenetic alopecia mice (AGA/Gas6) and 5% minoxidil treated androgenetic alopecia mice (AGA/Minoxidil). (A) Mouse skin color score index. (B) Hair weight was shaved from the same area in dorsal skin from different groups with a precision balance on Day 26. (C) Quantification of the skin color scores in mice based on the mouse skin color score. (D) Fluorescence images of frozen mouse skin tissue sections after treatment with Gas6-mcherry plasmid loaded complexes. Scale bar = 100 μm (E) H&E staining images of dorsal skin paraffin sections with different treatments. Green arrows represent vellus hairs and red arrows represent terminal hairs. Scale bar = 250 μm. (F) Immunofluorescence images of the TUNEL apoptosis assay (scale bar = 50 μm) and immunohistochemistry staining images of the proliferation marker ki67 (scale bar = 500 μm). (G) Gas6 mRNA expression was quantified via RT-qPCR at the topical administration sites. (H) Western blotting of Gas6, p-STAT3, STAT3, Bcl-2 and β-actin expression in skin. (I), (J) and (K) represent the quantification of Gas6, p-STAT3 and Bc l-2 protein expression via ImageJ software. Data are shown as mean ± SEM ($n \geq 3$; unpaired two-tailed Student's *t*-test; *$p < 0.05$; **$p < 0.01$; ***$p < 0.001$). (For interpretation of the references to colour in this figure legend, the reader is referred to the Web version of this article.)

treatment group stimulated STAT3 phosphorylation and further activated the antiapoptotic protein Bcl-2, thereby inhibiting the apoptosis of hair follicle cells, prolonging the anagen status, promoting the proliferation and differentiation of hair follicle cells, and finally alleviating the symptoms of androgenetic alopecia in mice.

4. Conclusions

Transdermal penetration of functional nucleic acids is extremely important for the treatment of skin-related diseases such as androgenetic alopecia. A new gene delivery vector is necessary for efficient transdermal administration. In this work, these PEI-Triton-N conjugates with different numbers of Triton X-100 per PEI 1.8 kDa were rationally designed and synthesized, which showed higher cell transfection efficiency and lower cytotoxicity than PEI 25 kDa and Lipofectamine in most cell lines. PEI-Triton X-100 conjugates could obviously enhance the transmembrane efficiency for pDNAs in hard-to-transfect HaCaT cells as well as the transdermal transfection efficiency of DNA plasmids in a mouse model. PEI-Triton X-100 conjugates after topical administration did not induce the obvious redness, ulceration or allergy of skin as well as systemic toxicity of the organs, such as liver and kidney.

Further our results also lend new insight into the signaling of hair growth regulation in androgenetic alopecia mice. Androgenetic alopecia is a very common and tricky chronic skin-related disease that usually depended on androgens and is characterized by genetic patterns, but the action mechanism of androgenetic alopecia is not yet fully known. Previous report indicates that Gas6 is secreted by dermal papilla cells and can promote the proliferation of hair follicles and reverse stress-induced hair loss. However, whether Gas6 can reverse androgen hair loss has not been reported. Thus, we applied PEI-Triton-N conjugates and $pDNA_{Gas6}$ to form the stable PEI-Triton-6/$pDNA_{Gas6}$ complexes. Our mice studies indicated that these PEI-Triton-6/$pDNA_{Gas6}$ complexes could efficiently and safely deliver the Gas6 plasmid to hair follicles via transdermal administration in androgenetic alopecia mice. The overexpressed Gas6 further activated STAT3 phosphorylation and upregulated the expression of antiapoptotic protein Bcl-2, which resulted in the inhibition of the apoptosis of hair follicles, elongation of anagen status, promotion of the proliferation and differentiation of hair follicle cells, and further alleviation of the symptoms of androgenetic alopecia mice. These data indicate that Gas6 is a high-potential gene therapy candidate for the treatment of androgenetic alopecia with our transdermal gene delivery agents in future. With PEI-Triton-N conjugates as effective and safe reagents, their complexes with functional nucleic acids would provide a new strategy for gene therapy in skin-related diseases.

Credit author statement

Xinli Fan: Conceptualization, Methodology, Investigation, Data curation, Formal analysis, Writing- Original draft preparation. Xiaoran Zhao: Investigation and Data curation. Jianfei Xu: Validation, Resources. Jing Wang: Formal analysis, Writing-Reviewing and Editing. Qian Wang: Formal analysis, Writing-Reviewing and Editing. Xinjing Tang: Conceptualization, Supervision, Writing-Reviewing and Editing, Funding acquisition.

Declaration of competing interest

The authors declare that they have no known competing financial interests or personal relationships that could have appeared to influence the work reported in this paper.

Data availability

Data will be made available on request.

Acknowledgments

This work was financially supported by the National Natural Science Foundation of China (Grants No. 81821004, 22207006, 22077005, 21877001) and the open fund of the state key laboratory of Pharmaceutical Biotechnology, Nanjing University, China (Grant No. KF-202205).

Appendix A. Supplementary data

Supplementary data to this article can be found online at https://doi.org/10.1016/j.mtbio.2023.100575.

References

[1] F. Lolli, F. Pallotti, A. Rossi, M.C. Fortuna, G. Caro, A. Lenzi, A. Sansone, F. Lombardo, Androgenetic alopecia: a review, Endocrine 57 (1) (2017) 9–17.
[2] K.S. Houschyar, M.R. Borrelli, C. Tapking, D. Popp, B. Puladi, M. Ooms, M.P. Chelliah, S. Rein, D. Pforringer, D. Thor, G. Reumuth, C. Wallner, L.K. Branski, F. Siemers, G. Grieb, M. Lehnhardt, A.S. Yazdi, Z.N. Maan, D. Duscher, Molecular mechanisms of hair growth and regeneration: current understanding and novel paradigms, Dermatology 236 (4) (2020) 271–280.
[3] Yingzi Liu, F. Christian, Guerrero-Juarez, Fei Xiao, , Nitish Udupi Shettigar, Raul Ramos, Chen-Hsiang Kuan, Yuh-Charn Lin, , Luis de Jesus Martinez Lomeli, Jung Min Park, Ji Won Oh, Ruiqi Liu, Sung-Jan Lin, Marco Tartaglia, Ruey-Bing Yang, Zhengquan Yu, Qing Nie, M.V. Ji Li, Plikus, Hedgehog signaling reprograms hair follicle niche fibroblasts to a hyper-activated state, Dev. Cell 57 (14) (2022) 1758.
[4] S.A. Lee, K.N. Li, T. Tumbar, Stem cell-intrinsic mechanisms regulating adult hair follicle homeostasis, Exp. Dermatol. 30 (4) (2021) 430–447.
[5] A. Hagner, W. Shin, S. Sinha, W. Alpaugh, M. Workentine, S. Abbasi, W. Rahmani, N. Agabalyan, N. Sharma, H. Sparks, J. Yoon, E. Labit, J. Cobb, I. Dobrinski, J. Biernaskie, Transcriptional profiling of the adult hair follicle mesenchyme reveals R-spondin as a novel regulator of dermal progenitor function, iScience 23 (4) (2020), 101019.
[6] Y. Shwartz, M. Gonzalez-Celeiro, C.L. Chen, H.A. Pasolli, S.H. Sheu, S.M. Fan, F. Shamsi, S. Assaad, E.T. Lin, B. Zhang, P.C. Tsai, M. He, Y.H. Tseng, S.J. Lin, Y.C. Hsu, Cell types promoting goosebumps form a niche to regulate hair follicle stem cells, Cell 182 (3) (2020) 578–593, e19.
[7] T. Zhang, S. Cao, H. Yuan, S. Park, Alleviation of androgenetic alopecia with aqueous paeonia lactiflora and poria cocos extract intake through suppressing the steroid hormone and inflammatory pathway, Pharmaceuticals 14 (11) (2021) 1128.
[8] M. Bellan, M.G. Cittone, S. Tonello, C. Rigamonti, L.M. Castello, F. Gavelli, M. Pirisi, P.P. Sainaghi, Gas6/TAM system: a key modulator of the interplay between inflammation and fibrosis, Int. J. Mol. Sci. 20 (20) (2019) 5070.
[9] M. Tanaka, D.W. Siemann, Gas6/Axl signaling pathway in the tumor immune microenvironment, Cancers 12 (7) (2020) 1850–1864.
[10] S. Choi, B. Zhang, S. Ma, M. Gonzalez-Celeiro, D. Stein, X. Jin, S.T. Kim, Y.L. Kang, A. Besnard, A. Rezza, L. Grisanti, J.D. Buenrostro, M. Rendl, M. Nahrendorf, A. Sahay, Y.C. Hsu, Corticosterone inhibits GAS6 to govern hair follicle stem-cell quiescence, Nature 592 (7854) (2021) 428–432.
[11] P. Suchonwanit, S. Thammarucha, K. Leerunyakul, Minoxidil and its use in hair disorders: a review, Drug Des. Dev. Ther. 13 (2019) 2777–2786.

[12] D.A. Whiting, Advances in the treatment of male androgenetic alopecia - a brief review of finasteride studies, Eur. J. Dermatol. 11 (4) (2001) 332–334.
[13] D.D. Nguyen, P. Herzog, E.B. Cone, M. Labban, K.C. Zorn, B. Chughtai, S. Basaria, D.S. Elterman, Q.D. Trinh, N. Bhojani, Disproportional signal of sexual dysfunction reports associated with finasteride use in young men with androgenetic alopecia: a pharmacovigilance analysis of VigiBase, J. Am. Acad. Dermatol. S0190–9622 (22) (2022), 00527-00528.
[14] J.A. Kulkarni, D. Witzigmann, S.B. Thomson, S. Chen, B.R. Leavitt, P.R. Cullis, R. van der Meel, The current landscape of nucleic acid therapeutics, Nat. Nanotechnol. 16 (6) (2021) 630–643.
[15] Q.U. Ain, E.V.R. Campos, A. Huynh, D. Witzigmann, S. Hedtrich, Gene delivery to the skin - how far have we come? Trends Biotechnol. 39 (5) (2021) 474–487.
[16] L.V. Depieri, L.N. Borgheti-Cardoso, P.M. Campos, K.K. Otaguiri, F.T. Vicentini, L.B. Lopes, M.J. Fonseca, M.V. Bentley, RNAi mediated IL-6 in vitro knockdown in psoriasis skin model with topical siRNA delivery system based on liquid crystalline phase, Eur. J. Pharm. Biopharm. 105 (2016) 50–58.
[17] M. Qin, G. Du, X. Sun, Recent advances in the noninvasive delivery of mRNA, Acc. Chem. Res. 54 (23) (2021) 4262–4271.
[18] F. Saviano, T. Lovato, A. Russo, G. Russo, C.R. Bouton, R.J. Shattock, C. Alexander, F. Quaglia, A.K. Blakney, P. Gurnani, C. Conte, Ornithine-derived oligomers and dendrimers for in vitro delivery of DNA and ex vivo transfection of skin cells via saRNA, J. Mater. Chem. B 8 (22) (2020) 4940–4949.
[19] S.K. Tripathi, Z. Ahmadi, K.C. Gupta, P. Kumar, Polyethylenimine-polyacrylic acid nanocomposites: type of bonding does influence the gene transfer efficacy and cytotoxicity, Colloids Surf. B Biointerfaces 140 (2016) 117–120.
[20] Z. Chen, Z. Lv, Y. Sun, Z. Chi, G. Qing, Recent advancements in polyethyleneimine-based materials and their biomedical, biotechnology, and biomaterial applications, J. Mater. Chem. B 8 (15) (2020) 2951–2973.
[21] D.N. Meenakshi Sundaram, S. Plianwong, R. Kc, H. Ostergaard, H. Uludag, Vitro cytotoxicity and cytokine production by lipid-substituted low molecular weight branched PEIs used for gene delivery, Acta Biomater. 148 (2022) 279–297.
[22] B. Thapa, S. Plianwong, K.C. Remant Bahadur, B. Rutherford, H. Uludag, Small hydrophobe substitution on polyethylenimine for plasmid DNA delivery: optimal substitution is critical for effective delivery, Acta Biomater. 33 (2016) 213–224.
[23] L.L. Ma, Q. Tang, M.X. Liu, X.Y. Liu, J.Y. Liu, Z.L. Lu, Y.G. Gao, R. Wang, [12] aneN3-Based gemini-type amphiphiles with two-photon absorption properties for enhanced nonviral gene delivery and bioimaging, ACS Appl. Mater. Interfaces 12 (36) (2020) 40094–40107.
[24] Q. Guo, Y.H. Liu, M.M. Xun, J. Zhang, Z. Huang, X.D. Zhou, X.Q. Yu, Diol glycidyl ether-bridged low molecular weight PEI as potential gene delivery vehicles, J. Mater. Chem. B 3 (13) (2015) 2660–2670.
[25] X. Fan, X. Zhao, W. Su, X. Tang, Triton X-100-modified adenosine triphosphate-responsive siRNA delivery agent for antitumor therapy, Mol. Pharm. 17 (10) (2020) 3696–3708.
[26] U. Griesenbach, C. Meng, R. Farley, M.Y. Wasowicz, F.M. Munkonge, M. Chan, C. Stoneham, S.G. Sumner-Jones, I.A. Pringle, D.R. Gill, S.C. Hyde, B. Stevenson, E. Holder, H. Ban, M. Hasegawa, S.H. Cheng, R.K. Scheule, P.L. Sinn, P.B. McCray Jr., E.W. Alton, The use of carboxymethylcellulose gel to increase non-viral gene transfer in mouse airways, Biomaterials 31 (9) (2010) 2665–2672.
[27] A. Qi, P. Chan, J. Ho, A. Rajapaksa, J. Friend, L. Yeo, Template-free synthesis and encapsulation technique for layer-by-layer polymer nanocarrier fabrication, ACS Nano 5 (12) (2011) 9583–9591.
[28] FDA, FDA Inactive Ingredient Databases, 2022.
[29] M. Yanagita, H. Arai, T. Nakano, K. Ohashi, K. Mizuno, A. Fukatsu, T. Doi, T. Kita, Gas6 induces mesangial cell proliferation via latent transcription factor STAT3, J. Biol. Chem. 276 (45) (2001) 42364–42369.
[30] H.J. Choi, J.S. Han, Overexpression of phospholipase D enhances Bcl-2 expression by activating STAT3 through independent activation of ERK and p38MAPK in HeLa cells, Biochim. Biophys. Acta 1823 (6) (2012) 1082–1091.